

Optimal Path Planning for Connected and Automated Vehicles in Lane-free Traffic

Venkata Karteek Yanumula, Panagiotis Typaldos, Dimitrios Troullinos, Milad Malekzadeh, Ioannis Papamichail, Markos Papageorgiou, *Life Fellow, IEEE*.

Abstract—This paper develops a path planning algorithm for Connected and Automated Vehicles (CAVs) driving on a lane-free highway, according to a recently proposed novel paradigm for vehicular traffic in the era of CAVs. The approach considers a simple model of vehicle kinematics, along with appropriate constraints for control variables and road boundaries. Appropriate, partly competitive sub-objectives are designed to enable efficient vehicle advancement, while avoiding collisions with other vehicles and infeasible vehicle maneuvers. Based on these elements, a nonlinear Optimal Control Problem (OCP) is formulated for each ego vehicle, and a Feasible Direction Algorithm (FDA) is employed for its computationally efficient numerical solution. The OCP is solved repeatedly for short time horizons within a Model Predictive Control (MPC) framework, while the vehicle advances. It is demonstrated via traffic simulation, involving many such vehicles, on a lane-free ring-road that the proposed approach delivers promising results and can be considered as a candidate for use in further developments related to lane-free CAV traffic.

Index Terms—Lane-free traffic, automated vehicles, optimal control, path planning, model predictive control.

I. INTRODUCTION

Automation in manufacturing, process control and further areas increased the productivity and minimized the errors to a great extent. Similar outcomes of high efficiency and increased safety are expected with automation in road vehicle driving. Human driving is limited with perception of senses, reaction time and decision making quality. Variations in the driving behaviour from person to person, in addition to mentioned limitations, may result in accidents and reduced utilization of the road infrastructure. In fact, the vast majority of road accidents are attributed to human error on the account of, e.g., insufficient sensory information, lack of attention, shortcomings in driving skill or reckless driving. Each year, road accidents result in approximately 1.35 million fatalities and leave some 50 million of injured or disabled worldwide. Road congestion is another major issue, causing excessive delays, fuel consumption and emissions [1], [2].

Despite some improvements, road accidents and road congestion persist as major societal problems, even after decades of research and developments in road safety and traffic management, and call for comprehensive solutions. Automated vehicles, aided by Vehicle-to-Vehicle (V2V) and

Vehicle-to-Infrastructure (V2I) communication, have the potential to substantially improve the road safety and optimize the traffic flow [3], [4]. Recent developments on sensors and communications deliver the systems onboard with high-quality and comprehensive information, which is processed to enable safer and more efficient driving compared to manual driving. Several metro lines across the world are operating automatically for safety, efficiency, and economic reasons. However, due to the complex nature of road traffic compared to railways, automation on roads needs more sophisticated algorithms, such as optimal control methods, advanced feedback control or reinforcement learning approaches [5], [6].

Lane-based traffic was introduced to simplify the driving task for human drivers; when driving on a lane, the driver needs to monitor only the distance and speed of the front vehicle, with no need to also monitor the vehicle's left, right and rear sides. On the other hand, lane-changing is more complex and risky, and it is indeed responsible for 10% of all road accidents [7]. Given the variation of vehicle widths (cars, vans, trucks, buses, motorcycles), as well as the need for safety margins, lane-based traffic is necessarily wasting a part of the available road width, and hence of potentially achievable capacity. Additional capacity losses occur due to dynamic phenomena attributed to lane-changing maneuvers, including the triggering of traffic breakdown at critical traffic conditions, because of the abrupt and space-consuming lateral displacements required in lane-based traffic.

Lane changing or overtaking is a high-risk and difficult task even for CAVs [8], [9], where trajectory calculations may be computationally heavy, with large amount of data, requiring various simplifications and assumptions. Optimal control and model predictive control (MPC) have been proposed to generate trajectories for lane-based traffic [10], [11], but the discrete character of lane changing calls for the introduction of corresponding discrete variables, which is a burden for real-time feasible solutions.

According to a recently proposed novel traffic paradigm [12], there is no need, in the era of high-level vehicle automation and connectivity, to mimic the human lane-based driving task. The future driving on roads is going in the direction of full automation, which necessitates the nurturing of novel ideas that simplify or remove unnecessarily restrictive traffic rules designed for human drivers. Vehicle sensors and communications enable a CAV to monitor simultaneously, continuously and reliably its surroundings on a 360° basis; and to make fast (computer-based) and efficient moving

The research leading to these results has received funding from the European Research Council under the European Union's Horizon 2020 Programme / ERC Grant Agreement no. 833915, project TrafficFluid, see: <https://www.trafficfluid.tuc.gr>

All the authors are with Dynamic Systems and Simulation Laboratory, Technical University of Crete, Chania, Crete, 73100, Greece, e-mail: {karteek, ptypaldos, dtroullinos, mmalek, ipapa, markos}@dssl.tuc.gr

decisions. These superbly increased capabilities, compared to human driving, allow for a CAV to “float” safely and efficiently in a stream of other, potentially cooperating, CAVs, based on appropriate movement strategies. Thus, highways, motorways, arterials, and even urban roads may attain a lane-free structure, regaining the lost capacity and also improving on traffic safety. Vehicle movement strategies for CAVs are easier to design, safer and more efficient in a lane-free environment due to smooth 2-D vehicle movement, where accident-prone, hence conservative, laterally “discontinuous” displacements to other lanes become obsolete.

This paper proposes a nonlinear constrained Optimal Control Problem (OCP) for CAV path planning in lane-free traffic, using only real-valued variables, thanks to the absence of pre-specified traffic lanes. In view of various possible unpredictable disturbances and the need for computational feasibility in real time, relatively short time horizons (8 s) are considered. Using an efficient Feasible Direction Algorithm (FDA) [13], the OCP is solved in 12.4 ms on average. This allows for repeated problem solution, with updated data of the dynamically changing environment, in the frame of an MPC approach. MPC has a long history of applications in control, automation, and chemical industries [14], [15], among others. One approach is to solve the OCP at each time step, with corresponding shift of the planning horizon. An alternative approach is to re-solve the OCP event-based [16], which is pursued in the current study.

The communication system for connected vehicles is not completely foolproof, in terms of cyberattacks or loss of data, but developments are on-going to render it more robust [17]. In the current study, it is assumed that V2V communication enables CAVs, within a limited road range, to share information related to their current state and short-term future trajectory.

The rest of the article is organized as follows: Section II presents the dynamics of each ego vehicle, the constraints and the components of the objective function that lead to the OCP formulation; it also includes an outline of the numerical solution algorithm. Section III explains the procedure used for MPC, along with simulation results for multiple vehicles driving on a ring-road. Section IV contains concluding remarks and outlines on-going work.

II. OPTIMAL CONTROL PROBLEM (OCP) AND NUMERICAL SOLUTION

The considered OCP comprises a dynamic system model, control bounds and an objective function, whose minimization reflects the achievement of a number of pursued objectives and behavioral features. These elements are described in the present section, concluding with the formulation of the OCP. Since all data handling in real time is to be executed in a digital computer onboard each vehicle and is time-discrete by nature, a discrete-time OCP formulation and model of vehicle kinematics are considered for the current work.

A. Vehicle Dynamics and Constraints

Each ego vehicle is described by four state equations, specifically two equations in each of the longitudinal and

lateral directions. The position of the ego vehicle is considered on a two-dimensional plane. The vehicle is controlled by the respective accelerations in the longitudinal and lateral directions. The lane-free concept of [12] allows for the use of real-valued states and controls, in particular a continuous positioning of vehicle in the lateral direction within the road boundaries. The dynamics of the vehicle in discrete time are described as follows:

$$x_1(k+1) = x_1(k) + Tx_3(k) + \frac{1}{2}T^2u_1(k) \quad (1a)$$

$$x_2(k+1) = x_2(k) + Tx_4(k) + \frac{1}{2}T^2u_2(k) \quad (1b)$$

$$x_3(k+1) = x_3(k) + Tu_1(k) \quad (1c)$$

$$x_4(k+1) = x_4(k) + Tu_2(k) \quad (1d)$$

where T is the step size; k is the discrete integer index, related to time t via $t = kT$; the states x_1, x_2, x_3, x_4 are longitudinal position (of the vehicle centre), lateral position (of the vehicle centre), longitudinal speed, lateral speed respectively; while u_1 and u_2 are control inputs that correspond to longitudinal and lateral accelerations, respectively. The use of the simple model (1) is justified by the fact that vehicles are essentially moving longitudinally, with very small heading angles, hence longitudinal and lateral movement may be considered to be decoupled. In addition, an appropriate term in the objective function discourages vehicle paths that might be infeasible with vehicle steering.

Both accelerations are bounded, whereby the longitudinal upper bound is constant, while the longitudinal lower bound and the lateral bounds are state-dependent, as follows

$$u_{\min 1}(x_3) \leq u_1(k) \leq u_{\max 1} \quad (2a)$$

$$u_{\min 2}(x_2, x_4) \leq u_2(k) \leq u_{\max 2}(x_2, x_4) \quad (2b)$$

The constant upper bound $u_{\max 1}$ of the longitudinal acceleration may be set with consideration of the vehicle capabilities and the passenger convenience. Furthermore, a vehicle, having a non-negative speed $x_3(k)$, should not have negative longitudinal speed at the next time step, i.e.

$$x_3(k+1) \geq 0 \quad (3)$$

should hold. To avoid state constraints that may complicate the numerical solution of the OCP, we replace the state equation (1c) in (3) and we obtain, after rearrangement,

$$u_1(k) \geq -\frac{1}{T}x_3(k) \quad (4)$$

This bound may be unrealistically low (negative) at higher speeds, due to the magnitude of the coefficient $-1/T$, which can be a cause of discomfort for the passengers. Note that the equation-version of (4) may be interpreted as a dead-beat controller that drives the speed x_3 to zero in exactly one time step. However, we can mitigate the magnitude of the resulting acceleration bounds by choosing a more moderate “controller” coefficient $0 < K_{\text{long}} \leq 1/T$, which would drive x_3 to zero asymptotically. This way, we obtain accordingly moderate lower acceleration bounds, while guaranteeing that the constraint (3) is always satisfied. In conclusion, the lower bound on longitudinal acceleration is selected to be,

$$u_{\min 1}(x_3(k)) = -K_{\text{long}}x_3(k) \quad (5)$$

and (2a) is replaced by the following state-dependent constraint to be considered in OCP,

$$h_1 = [u_1(k) - u_{\max 1}][u_1(k) - u_{\min 1}] \leq 0 \quad (6)$$

Regarding the lateral constraints (2b), the ego vehicle must stay within the lateral road boundaries, which, for the present study, are assumed to be straight lines. The vehicle, positioned within road boundaries laterally at $x_2(k)$ and $x_2(k+1)$ should not cross the road boundaries at time step $k+2$ i.e. we must have,

$$e_w \leq x_2(k+2) \leq r_w - e_w \quad (7)$$

where r_w is the road width, and e_w is half of the ego vehicle width. To avoid complications with state constraints in the numerical solution of the OCP, we prefer again to consider appropriate state-dependent control constraints. Note that, if the vehicle actually reaches the left or right road boundary, i.e. if the left or right constraint above is activated, then we must have for the lateral speed $x_4(k+2) = 0$, as otherwise the vehicle would eventually exit the road. By replacing state equations (1b) and (1d) in (7), it may be seen, after some rearrangements that the above constraints are satisfied via the following state-dependent inequalities for the lateral acceleration,

$$\begin{aligned} -\frac{1}{T^2}[x_2(k) - e_w] - \frac{3}{2T}x_4(k) &\leq u_2(k) \leq \\ &-\frac{1}{T^2}[x_2(k) - r_w + e_w] - \frac{3}{2T}x_4(k) \end{aligned} \quad (8)$$

Similar to (4) above, the state-dependent bounds in (8) may take very high magnitudes, which could be unrealistic or cause discomfort to the passengers. Note here also, that either part of (8), taken as equalities, may be interpreted as a respective dead-beat controller (depending on lateral position and speed) that drives the lateral position x_2 to the respective road boundary and the lateral speed x_4 to zero in exactly two time steps. However, we can mitigate the magnitude of the resulting acceleration bounds by choosing more moderate ‘‘controller’’ gains, so as to keep lateral acceleration within a comfortable range. Specifically the state-dependent bounds on lateral control may be generalized as,

$$\begin{aligned} u_{\min 2}(x_2(k), x_4(k)) &= -K_{\text{lat1}}[x_2(k) - e_w] \\ &\quad - K_{\text{lat2}}x_4(k) \end{aligned} \quad (9a)$$

$$\begin{aligned} u_{\max 2}(x_2(k), x_4(k)) &= -K_{\text{lat1}}[x_2(k) - r_w + e_w] \\ &\quad - K_{\text{lat2}}x_4(k) \end{aligned} \quad (9b)$$

where $0 < K_{\text{lat1}} \leq 1/T^2$ and $0 < K_{\text{lat2}} \leq 3/(2T)$ are feedback controller gains for the system (1b) and (1d) that may be chosen appropriately to prevent road departures by the ego vehicle via asymptotic approaching of the road boundaries. Specifically, by setting $K_{\text{lat2}} = 2\sqrt{K_{\text{lat1}}} - K_{\text{lat1}}T/2$, we get two identical poles of the closed-loop system, which may be placed, by the choice of K_{lat1} within the above range, anywhere on the positive real axis, so as to have an asymptotic behavior with accordingly moderate lateral acceleration. This way, we obtain moderate lateral acceleration bounds, while guaranteeing that the constraint (7) is always satisfied. In

conclusion, the following single inequality constraint, based on (9), is replacing (2b) in the OCP formulation,

$$h_2 = [u_2(k) - u_{\max 2}][u_2(k) - u_{\min 2}] \leq 0 \quad (10)$$

B. Objective Function

The objective function is designed to consider a number of different and partly competitive aspects regarding the moving behavior of the vehicle, such as driving at a desired longitudinal speed, considering passenger comfort, avoiding obstacles, and more. Each aspect is reflected in a corresponding sub-objective, and the overall objective is a weighted sum of the sub-objectives. Each sub-objective is a function of problem variables and possibly external variables and is required to be continuous and differentiable for good performance of the numerical solution algorithm used to solve the OCP. More specifically, the overall objective reflects the following aspects.

1) *Fuel Consumption and Passenger Comfort*: Fuel consumption, and hence also emissions, are reduced if longitudinal acceleration maneuvers are mitigated. A quadratic cost term of longitudinal acceleration acts as an excellent proxy for minimizing the fuel consumption, as demonstrated in [18]. Thus, this sub-objective is considered by minimizing the quadratic terms $(u_1(k))^2$. Moreover, the quadratic terms lead to smooth acceleration and deceleration over time in both longitudinal and lateral directions, which benefits passenger comfort, hence we also include a quadratic term $(u_2(k))^2$ for the lateral acceleration.

2) *Desired Speed*: The ego vehicle is expected to drive, if the traffic conditions allow, at pre-specified desired speeds on both longitudinal and lateral directions. This is achieved by penalising the quadratic terms $(x_3(k) - v_{d_1})^2$ and $(x_4(k) - v_{d_2})^2$, where v_{d_1} and v_{d_2} are the desired speeds on longitudinal and lateral directions. In the current study, v_{d_1} has a positive value, while v_{d_2} is set to zero to minimize the lateral movement on straight roads. Obviously, the efficiency of advancing for the vehicle depends on its capability to drive with longitudinal speed close to the desired one, something that may of course be hindered in cases of dense traffic conditions around the vehicle.

3) *Avoidance of Obstacles*: An ego vehicle treats other vehicles in its neighbourhood as obstacles. To this end, an *interaction zone* around the ego vehicle is specified, comprising two parts, one downstream and another upstream of the ego vehicle. Both parts have the same length, which equals the product of the longitudinal desired speed times the planning horizon; and all vehicles included in the interaction zone are treated as obstacles by the ego vehicle. It is assumed that vehicles communicate and share their decisions. Thus, each ego vehicle knows about the latest decided future trajectories of all its obstacles, though this prediction may not be accurate, as decisions of the obstacles may have to be updated according to MPC (see Section III-A)

The distance of an automated vehicle from the preceding vehicle, in lane-based driving, follows commonly the constant time-gap (CTG) policy, whereby the distance is a linear

function of the follower's speed, and the proportionality factor is a design parameter, known as the time-gap. Time-gap-like design parameters $(\omega_{x_1}, \omega_{x_2})$, now in both longitudinal and lateral directions, are used also in this work, along with the vehicles' physical dimensions, to specify safe distances for all speed ranges in both moving directions in lane-free traffic. Consider there are n obstacles inside the interaction zone of an ego vehicle, and i^{th} obstacle's relative position (of obstacle centre) and speed are (o_{i1}, o_{i2}) and (o_{i3}, o_{i4}) respectively. The ego vehicle considers the safe distance around the obstacle based on a cost function in the form of a positive-valued ellipsoid, appropriately designed.

The basis to construct the ellipsoid is the design of an ellipse surrounding the obstacle. The dimensions and positioning of the ellipse in longitudinal direction are specified based on the following requirements:

- A safe space-gap, equal to $\omega_{x_1} x_3$, should be maintained between ego vehicle and obstacle when the ego vehicle is behind the obstacle.
- A safe space-gap, equal to $\omega_{x_1} o_{i3}$, should be maintained between ego vehicle and obstacle when the ego vehicle is in front of the obstacle. This gap prevents the ego vehicle from moving dangerously close in front of the obstacle (cut-in). It is interesting to note that this gap acts as "nudging" of the ego vehicle by the obstacle in the sense of [12].
- Physical dimensions of both ego and obstacle vehicles along with some safety margins, should be considered at zero speed. To this end, we define $L_i = l_e + l_{oi}$, where l_e and l_{oi} are 1.8 times the lengths of ego and obstacle vehicles, respectively.

These requirements are fulfilled, if the longitudinal ellipse axis is set $s_{d_1} = L_i + \omega_{x_1} x_3 + \omega_{x_1} o_{i3}$, while the ellipse's longitudinal center is positioned at

$$\delta_{o_1} = o_{i1} - \omega_{x_1} (x_3 - o_{i3}) / 2 \quad (11)$$

The handling of obstacles in lateral direction is slightly different, as time-gaps and safe distances depending on lateral speeds are considered only when the vehicles are approaching each other. Since lateral speeds may be positive or negative, the safe space-gap is $\omega_{x_2} |x_4 - o_{i4}|$ and it applies only when the vehicles are approaching each other; else it is zero. A smoothified function of the lateral ellipse axis, including the vehicle widths, reads

$$s_{d_2} = W_i + \omega_{x_2} \left[\tanh(o_{i2} - x_2) (x_4 - o_{i4}) + \sqrt{[\tanh(o_{i2} - x_2) (x_4 - o_{i4})]^2 + \epsilon_w} \right] \quad (12)$$

where $W_i = w_e + w_{oi}$, with w_e and w_{oi} being 1.3 times the respective widths of ego and obstacle vehicles, respectively. The lateral midpoint of the ellipse coincides with the center of the obstacle in lateral direction. The safety factors 1.8 and 1.3 on longitudinal and lateral directions, respectively, are chosen to ensure that the physical dimensions, in particular also the corners, of the rectangular-shaped vehicles are fully covered by the ellipse.

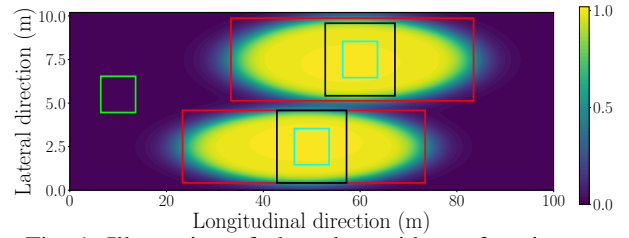


Fig. 1: Illustration of obstacle avoidance function

The ellipsoid function, used to construct a sort of potential function that penalizes the vehicle's approach to the obstacle and acts as a collision avoidance term, is as follows

$$c_i(x, o_i) = \frac{1}{\left[\left(\frac{x_1 - \delta_{o_1}}{0.5 s_{d_1}} \right)^{p_1} + \left(\frac{x_2 - o_{i2}}{0.5 s_{d_2}} \right)^{p_2} \right]^{p_3} + 1} \quad (13)$$

where p_1 and p_2 are positive even integers and p_3 is a positive integer. Thus, the ego vehicle "sees" each obstacle as an ellipsoid hemisphere, based on the specified longitudinal axis s_{d_1} , lateral axis s_{d_2} and unity value height. The sub-objective function to avoid n obstacles is then $\sum_{i=1}^n [c_i(x, o_i)]$.

As an illustrative example, a contour plot of penalty functions related to obstacle avoidance is shown in Fig. 1. One ego vehicle and two obstacles are considered, and all vehicles are 5 m long and 2 m wide. The ego vehicle is positioned at (10, 5.5) m with speeds (30.0, 1.5) m/s and is marked with a green box. Two obstacles 1 and 2 are positioned at (50, 2.5) m and (60, 7.5) m with speeds (25.0, 0.0) m/s and (25.0, 0.0) m/s, respectively, and are marked with cyan boxes. The time-gaps $(\omega_{x_1}, \omega_{x_2})$ are (0.5, 0.25) s. The augmented dimensions, including the ego and obstacle vehicles' dimensions are depicted by black boxes, and the ellipsoid dimensions are represented by red boxes. Note that the red boxes of both obstacles are shifted towards the ego vehicle due to difference in longitudinal speeds. The width of the red box of obstacle 1 coincides with that of the black box, because both vehicles are laterally diverging. In contrast, the red box of obstacle 2 has increased width, compared to the black box, because the ego vehicle is approaching the obstacle laterally. The figure displays the space-dependent height of the ellipsoid with parameters $p_1 = 2$, $p_2 = 2$, $p_3 = 6$. Notice the fading width of the ellipsoid, which facilitates ego vehicle movement around the obstacle at higher ego vehicle speeds.

4) *Coupling of Longitudinal and Lateral Speeds:* The vehicle dynamics in (1) describe decoupled longitudinal and lateral movements. In extreme cases, particularly at very low longitudinal speeds, this simplified model may lead to unrealistic or infeasible maneuvers for the real vehicle, e.g. a vehicle moving only laterally ($x_3(k) = 0$ and $x_4(k) \neq 0$). In order to prevent such situations, the following sub-objective with some small $\beta > 0$ is considered,

$$f_c = \begin{cases} (\beta x_3(k) - x_4(k))^2 & \text{if } x_4(k) > \beta x_3(k) \\ (\beta x_3(k) + x_4(k))^2 & \text{if } x_4(k) < -\beta x_3(k) \\ 0 & \text{otherwise} \end{cases} \quad (14)$$

The magnitude of f_c increases quadratically if the magnitude of lateral speed is greater than β times the magnitude of

longitudinal speed. Minimization of the sub-objective (14) couples indirectly the vehicle movements in longitudinal and lateral directions, when needed.

C. Optimal Control Problem Formulation

Considering all sub-objectives, the OCP is defined as minimization of the following objective criterion, subject to state equations (1) and control constraints (6) and (10),

$$J = \sum_{k=0}^{K-1} \left[w_1 (u_1(k))^2 + w_2 (u_2(k))^2 + w_3 (x_3(k) - v_{d_1})^2 + w_4 (x_4(k) - v_{d_2})^2 + w_5 \sum_{i=1}^n [c_i(\mathbf{x}, \mathbf{o}_i)] + w_6 f_c \right] \quad (15)$$

where w_1 to w_6 are weighting factors to be chosen appropriately; and K is the planning horizon. The general form of the objective function is given by

$$J = \sum_{k=0}^{K-1} \Phi[\mathbf{x}(k), \mathbf{u}(k)] \quad (16)$$

The general form of (1) is

$$\mathbf{x}(k+1) = \mathbf{f}[\mathbf{x}(k), \mathbf{u}(k)] \quad (17)$$

The Hamiltonian function is defined as

$$H[\mathbf{x}(k), \mathbf{u}(k), \boldsymbol{\lambda}(k+1), \boldsymbol{\mu}(k)] = \boldsymbol{\lambda}(k+1)^T \mathbf{f}[\mathbf{x}(k), \mathbf{u}(k)] + \Phi[\mathbf{x}(k), \mathbf{u}(k)] + \boldsymbol{\mu}(k)^T \mathbf{h}[\mathbf{x}(k), \mathbf{u}(k)] \quad (18)$$

where $\boldsymbol{\lambda}(k)$ are the co-states, associated with the state equations, and $\boldsymbol{\mu}(k)$ are multipliers, associated with the constraints. Based on these, the necessary conditions of optimality, to be used in the numerical solution algorithm, are given here. We have the state equation

$$\mathbf{x}(k+1) = \frac{\partial H}{\partial \boldsymbol{\lambda}(k+1)} = \mathbf{f}[\mathbf{x}(k), \mathbf{u}(k)] \quad (19)$$

We have the control condition

$$\partial H / \partial \mathbf{u}(k) = \mathbf{0} \quad (20)$$

The co-state equation is given by

$$\boldsymbol{\lambda}(k) = \partial H / \partial \mathbf{x}(k) \quad (21)$$

Finally, the boundary conditions are given by

$$\mathbf{x}(0) = \mathbf{x}_0 \quad (22a)$$

$$\boldsymbol{\lambda}(K) = \mathbf{0} \quad (22b)$$

D. Numerical Solution Algorithm

The solution of the described OCP must be obtained through an efficient numerical solver that enables real-time feasibility. A very efficient feasible direction algorithm (FDA) [13], [19] is employed to solve the present OCP. The algorithm utilizes the explicit structure of the state equations and exploits the necessary conditions of optimality to map the OCP into a Nonlinear Programming (NLP) problem in the reduced space of control variables. Thus, the algorithm attempts to reach a control trajectory $\mathbf{u}(k), k = 0, \dots, K-1$, which corresponds to a local minimum of the cost function in the mK -dimensional space, where m is the number of control variables. This marks a substantial reduction of the problem dimension, as the state variables are eliminated.

More specifically, FDA exploits the fact that $\mathbf{g}(k) = [\partial \mathbf{f} / \partial \mathbf{u}(k)]^T \boldsymbol{\lambda}(k+1) + \partial \Phi / \partial \mathbf{u}(k)$ equals the reduced gradient in the mK -dimensional reduced space of the control, if the states and co-states involved in the partial derivative satisfy the state and co-state equations. Having this possibility to calculate reduced gradients, FDA is an iterative procedure, starting with a feasible initial-guess control trajectory specified by the user. The algorithm can be readily extended, to consider bounds on the control variables [13], [19]. The multipliers of the inequality constraints (for $i = 1, 2$) that define bounds are calculated using (20), as, $\mu_i(k) = -g_i(k) / [\partial h_i / \partial u_i(k)]$ for active constraints and $\mu_i(k) = 0$ for inactive constraints. Each iteration employs an appropriate descent direction (e.g. conjugate gradients or quasi-Newton direction), to specify an improved control trajectory that reduces the objective function value, while satisfying the state equations and constraints. The improved control trajectory is the starting point of the next iteration, and so forth. The algorithm stops at a local minimum, when the gradient approaches sufficiently a zero value. It should be noted that an initial-guess trajectory that is closer to the optimal one may reduce the required number of iterations. The algorithmic steps are presented at Algorithm 1 (superscripts (l) indicate the iteration index).

Among several conjugate gradients and Quasi-Newton methods, the Fletcher-Reeves method was found most efficient for this OCP and is used for calculating search directions inside FDA. The approach is fast enough to be considered for real-time applications. With appropriate tuning of some algorithm parameters, the algorithm's runtime to generate vehicle paths, for a planning horizon of 8 s with a time-step size of $T = 250$ ms, is 12.4 ms on average (less than 100 ms in 99.9% plans, less than 250 ms in 99.99% plans) on a machine powered by Intel Core i5-8500 CPU operating at a maximum of 3.00 GHz frequency.

It should also be noted that FDA iterations may be stopped at any time, even before convergence, delivering a control trajectory that may not be the optimal one, but is feasible, i.e. satisfies all state equations and constraints. Last not least, as the OCP at hand is non-convex, FDA may converge to a local minimum. Although it is not possible to know, for any delivered minimum, whether it is a local or global one, we never identified in the extensive simulation investigations of Section III, any awkward ego vehicle maneuvers that might correspond to a bad local minimum.

Algorithm 1 Feasible Direction Algorithm

- 1: Receive initial values.
- 2: Guess an initial feasible control $\mathbf{u}^{(0)}(k), k = 0, \dots, K-1$.
- 3: Compute states $\mathbf{x}^{(0)}(k), k = 0, \dots, K-1$.
- 4: In a unique loop: compute $\mathbf{g}^{(0)}(k), \boldsymbol{\mu}^{(0)}(k)$ and co-states $\boldsymbol{\lambda}^{(0)}(k)$ for $k = K-1, \dots, 0$ starting with $\boldsymbol{\lambda}^{(0)}(K)$.
- 5: Set iteration index $l = 0$.
- 6: **while** $l < \text{maximum iterations}$ **do**
- 7: Compute a search direction $\mathbf{s}^{(l)}(k), k = 0, \dots, K-1$.
- 8: Compute a scalar step $\xi^{(l)}$ through line optimization.

- 9: Compute $\mathbf{u}^{(l+1)}(k) = \mathbf{u}^{(l)}(k) + \xi^{(l)} \mathbf{s}^{(l)}(k)$ and $\mathbf{x}^{(l+1)}(k)$ for $k = 0, \dots, K - 1$ (apply bounds on control).
- 10: In a unique loop: compute $\mathbf{g}^{(l+1)}(k)$, $\boldsymbol{\mu}^{(l+1)}(k)$, and co-states $\boldsymbol{\lambda}^{(l+1)}(k)$ for $k = K - 1, \dots, 0$ starting with $\boldsymbol{\lambda}^{(l+1)}(K)$.
- 11: Compute projected gradient when the control bounds are applied.
- 12: **if** not converged **then**
- 13: index increment, $l := l + 1$
- 14: continue
- 15: **else**
- 16: break
- 17: **end if**
- 18: **end while**
- 19: Generate control input $\mathbf{u}(k)$, $k = 0, \dots, K - 1$.

III. SIMULATION RESULTS WITH MODEL PREDICTIVE CONTROL (MPC)

A. Model Predictive Control (MPC)

The FDA algorithm is run to solve the OCP for finite time horizons of 8 s in an MPC framework. MPC is applied in emulated real time to all vehicles in the simulated scenario described below. Each ego vehicle receives, in an asynchronous mode, the decisions of all other vehicles in its neighborhood (its obstacles), as described in Section II-B.3, as well as their current states. If the currently available decision of an obstacle does not extend up to the whole planning horizon of the ego vehicle, then the ego vehicle extrapolates the received decision on the assumption of zero accelerations (longitudinally and laterally). The obstacle trajectories are used by the ego vehicle in the obstacle avoidance sub-objective of OCP. The MPC framework triggers a path re-planning, with updated initial state and obstacle movement prediction, event-based, as explained later.

Thus, each ego vehicle's OCP is solved based on its current initial state; the current states of the neighboring vehicles; and the available decided paths of the neighboring vehicles. To avoid unreasonable values of longitudinal acceleration at lower speeds due to the high cost resulting from a big difference between the current vehicle speed and the desired speed in longitudinal direction, the "running" desired speed v_{d_1} considered within the objective function at each planning is limited to 1.5 m/s above the current longitudinal speed. In addition, in cases of high vehicle density D_d (in veh/km) downstream of the ego vehicle, where fast advancing or overtaking is not possible, the running desired speed, is set equal to the average downstream longitudinal speed D_v added with 0.5 m/s. As a safety measure, the running desired speed is limited to an additional 1.5 m/s above current longitudinal speed even in high vehicle density cases. In summary, we have for the running desired speed

$$v_{d_1} = \begin{cases} x_3 + 1.5 & \text{if } D_d \leq D_{\min} \\ \min\{x_3 + 1.5, D_v + 0.5\} & \text{if } D_d > D_{\min} \end{cases} \quad (23)$$

This running desired speed v_{d_1} is truncated if it exceeds the actual desired speed of the corresponding ego vehicle.

The produced 8-s path of each ego vehicle is updated, according to the designed MPC procedure, i.e. the vehicle's OCP is re-solved online, if any of the following happens:

- The vehicle has been driving for 4 s according to the last generated trajectory; note that application of the full-horizon decisions may lead to myopic actions.
- Any of the dynamic obstacles (other vehicles) deviates substantially (0.2 m longitudinally or 0.1 m laterally) from its communicated or predicted path; note that this corresponds to inaccurate obstacle movement prediction that could lead to collisions.
- A new obstacle enters the interaction zone of the ego vehicle.

In any of these cases, the unused rest of the last ego vehicle control trajectory is used to obtain a good initial guess for the next FDA application, so as to reduce the algorithm's required iterations to converge; while for the rest of the guess trajectory, zero accelerations are used. Note that, in case of possible convergence difficulties, the FDA algorithm may be stopped at any time, since the trajectories produced at each iteration may be non-optimal, if convergence is not yet achieved, but are feasible, i.e. they satisfy the state equations and control bounds.

B. Simulation Environment

Simulations are performed using a custom extension of the SUMO (Simulation of Urban MObility) simulator [20], namely TrafficFluid-Sim [21], which extends the open-source codebase of SUMO to fit the need for lane-free simulation environments. Vehicle control was performed through an external application programming interface (API), that is integrated with TrafficFluid-Sim. As such, custom lane-free controllers are supported, with unified control over the longitudinal and lateral dimension, since the default SUMO car-following and lane-changing models are not appropriate for lane-free vehicle movement strategies.

Relevant functionalities include but are not limited to: initialization of the vehicles, support for multiple types of vehicles, controllers and parametrized penetration rates (when needed), online monitoring of loop detectors. The MPC framework is incorporated into the API and invokes the FDA algorithm when needed.

C. Simulated Scenario and Results

Eight classes of vehicles are considered, each class with its own dimensions (length, width) in m: (3.2, 1.6), (3.4, 1.7), (3.9, 1.7), (4.25, 1.8), (4.55, 1.82), (4.6, 1.77), (5.15, 1.84), and (5.2, 1.88). The desired speeds are assigned randomly with a uniform distribution between 25 m/s and 35 m/s.

A ring road of 1.0 km length, 10.2 m width, and, of course, a lane-free structure is considered for simulation. All the vehicles start from zero speed and strive to reach their longitudinal desired speed and a zero lateral desired speed. The following parameters are used for the simulations:

- In (16), $\{w_1, w_2, w_3, w_4, w_5, w_6\} = \{0.05, 0.05, 0.025, 0.05, 2, 0.1\}$.



Fig. 2: Simulation environment of SUMO

- Longitudinal safety time gap $\omega_{x_1} = 0.5$ s and lateral safety time gap $\omega_{x_2} = 0.25$ s, $\epsilon_w = 0.001$ in (12).
- In (13), $p_1 = p_2 = 2$ and $p_3 = 6$.
- In (14), $\beta = 0.03$.
- The discrete sample size is $T = 250$ ms. Time horizon is 8 s, hence $K = 32$.
- The distance range used for downstream density calculation in (23) is 150 m with $D_{\min} = 100$ veh/km.

Fig. 2 displays a snapshot from the related simulation video, where the ring-road is unfolded as a straight segment for simplicity. Various scenarios with different densities of up to 300 veh/km are considered and the related statistics are given in Table I.

TABLE I: Density (veh/km) and flow (veh/h) results

Density	50	100	150	200	250	300
Flow	5125	9592	12843	15478	14634	13728
β_{\max}	0.049	0.038	0.033	0.035	0.043	0.041

For a density of 100 veh/km (i.e. 100 vehicles driving on the ring-road of 1 km length) and a simulation time horizon of 20 min, an average flow of 9592 veh/h is achieved. Note that the road width suffices barely for 3 conventional traffic lanes, hence this flow is significantly higher than a conventional lane-based traffic capacity, which would not exceed 2,500 veh/h/lane. Note that, at 200 veh/km density, the flow reaches its highest value (capacity) at 14634 veh/h, before decreasing at higher density values. There no collisions reported in densities up to 300 veh/km.

The readings of β_{\max} in Table I correspond to the maximum value of the ratio of the magnitudes of lateral speed and longitudinal speed, excluding the very first planning horizon. Note that, due to the stochastic placement of vehicles and their zero speed at the start of simulation, the very first planning horizon can have artificially higher β values, but they were observed to be always less than 0.07.

Trajectories of two representative vehicles in the simulation are depicted in Figs. 3 to 6, corresponding vehicle movements in the SUMO simulator are available as videos at <https://bit.ly/2PvNCMB>. Note that, in the videos, the camera is tracking the particular vehicle of interest, whose movement can be matched with the trajectories presented in the figures. The surrounding vehicles appear to move forward if their relative longitudinal speed is greater than the one of the ego vehicles being tracked. Similarly, the surrounding vehicles appear to move back if their relative longitudinal speed is less than the one of the ego vehicles being tracked.

Recall that, at each path planning, the running desired longitudinal speed used in the OCP is limited by an additional

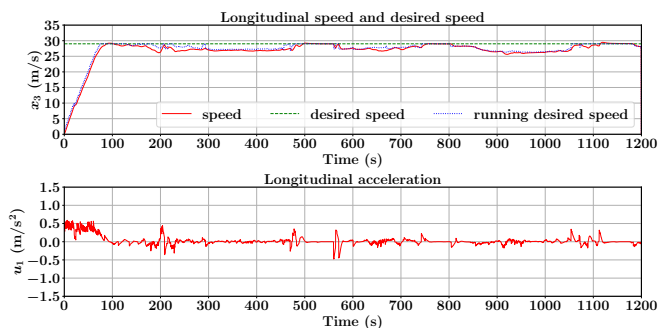


Fig. 3: Longitudinal movement in 100 veh/km density

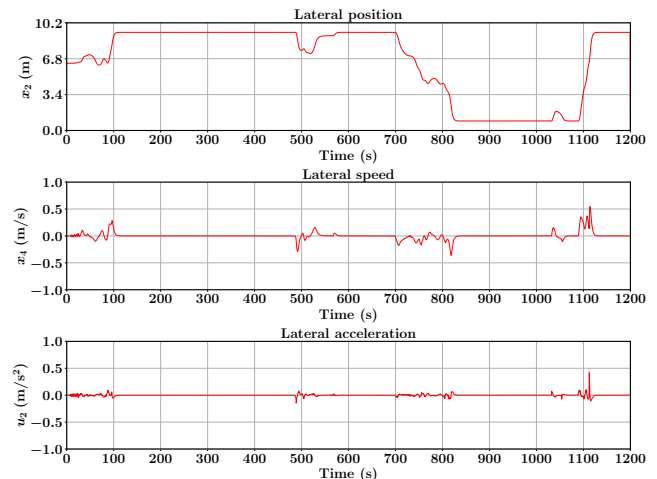


Fig. 4: Lateral movement in 100 veh/km density

1.5 m/s to the current longitudinal speed in accordance with (23). Figs. 3 and 5 display the desired longitudinal speed (green dashed line), the running desired longitudinal speed (blue dashed line) and the actual speed (red line). The vehicle starts from zero speed and reaches the desired longitudinal speed (Fig. 3) or it reaches some “steady state” speed depending on the obstacles around (Fig. 5). The accelerations are limited in magnitude and fairly smooth, which is good for passenger convenience and fuel consumption. In conclusion, actual longitudinal speed does not always reach or constantly stay at the desired speed due to fairly dense traffic conditions and other vehicles ahead, with lower desired speeds, that need to be overtaken.

The lateral movement is also seen to be influenced by surrounding density and space availability, as visible from the trajectories shown in Figs. 4 and 6. Specifically, at lower density (Fig. 4), the ego vehicle is seen to vividly change its lateral position, occasionally over the complete width of the road, in order to avoid or overtake other slower vehicles in front and advance faster; something that is not equally possible in higher density conditions (Fig. 6). In any case, the corresponding lateral speed and acceleration trajectories are moderate in magnitude and fairly smooth, which is good for the passenger convenience.

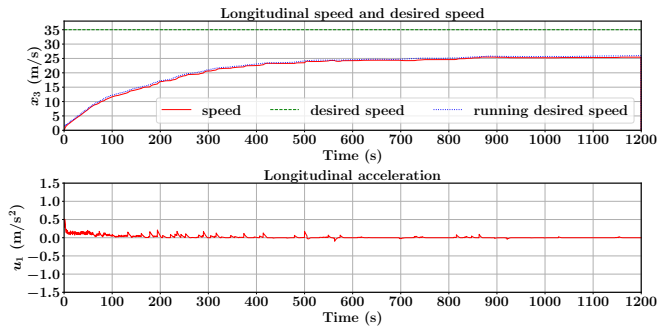


Fig. 5: Longitudinal movement in 200 veh/km density

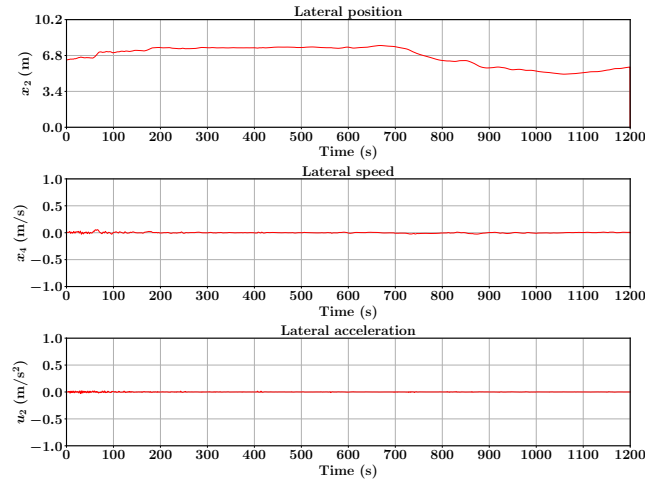


Fig. 6: Lateral movement in 200 veh/km density

IV. CONCLUSION

An optimal path-planning approach is developed for use in an event-triggered MPC mode for CAV in lane-free road environment. In the proposed approach, an appropriate OCP is formulated, taking into account efficiency, safety and convenience aspects, as well as road boundary and further constraints. The OCP is solved numerically with NLP techniques using an efficient FDA algorithm, which converges to a local minimum in polynomial time. The approach is applied simultaneously to multiple communicating vehicles, which share information about their states and movement decisions. MPC is run with a planning horizon of 8 s and is updated when significant deviations occur or when half of the horizon time has expired. It is demonstrated via simulation on a ring-road with hundreds of driving vehicles that the proposed approach leads to very efficient traffic flow, while preserving safety and passenger convenience.

Current and future work is focussed on:

- Improving the efficiency in terms of road utilization and flow maximization.
- Application of the algorithm in even further higher traffic densities.
- Introduction of state-dependent bounds on longitudinal control in emergency situations at high densities to avoid collisions.
- Introducing on-ramps, off-ramps and variable road widths.

REFERENCES

- [1] K. Goniewicz, M. Goniewicz, W. Pawłowski, and P. Fiedor, "Road accident rates: strategies and programmes for improving road traffic safety," *European Journal of Trauma and Emergency Surgery*, vol. 42, no. 4, pp. 433–438, 2016.
- [2] U. Montanaro, S. Dixit, S. Fallah, M. Dianati, A. Stevens, D. Oxtoby, and A. Mouzakitis, "Towards connected autonomous driving: review of use-cases," *Vehicle System Dynamics*, vol. 57, no. 6, pp. 779–814, 2019.
- [3] K. Sjöberg, P. Andres, T. Buburuzan, and A. Brakemeier, "Cooperative intelligent transport systems in Europe: Current deployment status and outlook," *IEEE Vehicular Technology Magazine*, vol. 12, no. 2, pp. 89–97, 2017.
- [4] C. Diakaki, M. Papageorgiou, I. Papamichail, and I. Nikolos, "Overview and analysis of vehicle automation and communication systems from a motorway traffic management perspective," *Transp. Research Part A: Policy and Practice*, vol. 75, pp. 147–165, 2015.
- [5] L. Claussmann, M. Revilloud, D. Gruyer, and S. Glaser, "A review of motion planning for highway autonomous driving," *IEEE Trans. on Intelligent Transp. Systems*, vol. 21, no. 5, pp. 1826–1848, 2020.
- [6] A. Haydari and Y. Yilmaz, "Deep reinforcement learning for intelligent transp. systems: A survey," *IEEE Trans. on Intelligent Transp. Systems*, pp. 1–22, 2020.
- [7] M. Rahman, M. Chowdhury, Y. Xie, and Y. He, "Review of microscopic lane-changing models and future research opportunities," *IEEE Trans. on Intelligent Transp. Systems*, vol. 14, no. 4, pp. 1942–1956, 2013.
- [8] V. Milanés, D. F. Llorca, J. Villagrà, J. Píez, C. Fernández, I. Parra, C. González, and M. A. Sotelo, "Intelligent automatic overtaking system using vision for vehicle detection," *Expert Systems with Applications*, vol. 39, no. 3, pp. 3362–3373, 2012.
- [9] B. Vanholme, D. Gruyer, B. Lusetti, S. Glaser, and S. Mammar, "Highly automated driving on highways based on legal safety," *IEEE Trans. on Intelligent Transp. Systems*, vol. 14, no. 1, pp. 333–347, 2013.
- [10] K. Makantasis and M. Papageorgiou, "Motorway path planning for automated road vehicles based on optimal control methods," *Transp. Research Record*, vol. 2672, no. 19, pp. 112–123, 2018.
- [11] P. Typaldos, M. Papageorgiou, and I. Papamichail, "Optimization-based path-planning for connected and non-connected automated vehicles," *arXiv:2104.06778 [eess.SY]*, 2021.
- [12] M. Papageorgiou, K. S. Mountakis, I. Karafyllis, I. Papamichail, and Y. Wang, "Lane-free artificial-fluid concept for vehicular traffic," *Proceedings of the IEEE*, vol. 109, no. 2, pp. 114–121, 2021.
- [13] M. Papageorgiou, M. Marinaki, P. Typaldos, and K. Makantasis, "A feasible direction algorithm for the numerical solution of optimal control problems—extended version," *Chania, Greece: Technical University of Crete, Dynamics Sysyems and Simulations Laboratory*, pp. 2016–26, 2016.
- [14] D. Q. Mayne and H. Michalska, "Receding horizon control of non-linear systems," *IEEE Trans. on Automatic Control*, vol. 35, no. 7, pp. 814–824, 1990.
- [15] D. Q. Mayne, "Model predictive control: Recent developments and future promise," *Automatica*, vol. 50, no. 12, pp. 2967–2986, 2014.
- [16] Y. Khazaeni and C. G. Cassandras, "Event-driven cooperative receding horizon control for multi-agent systems in uncertain environments," *IEEE Trans. on Control of Network Systems*, vol. 5, no. 1, pp. 409–422, 2018.
- [17] J. Cui, L. S. Liew, G. Sabaliauskaite, and F. Zhou, "A review on safety failures, security attacks, and available countermeasures for autonomous vehicles," *Ad Hoc Networks*, vol. 90, p. 101823, 2019.
- [18] P. Typaldos, I. Papamichail, and M. Papageorgiou, "Minimization of fuel consumption for vehicle trajectories," *IEEE Trans. on Intelligent Transp. Systems*, vol. 21, no. 4, pp. 1716–1727, 2020.
- [19] M. Papageorgiou, M. Leibold, and M. Buss, *Optimierung: Statische, dynamische, stochastische Verfahren für die Anwendung*. Springer Berlin Heidelberg, 2015.
- [20] P. A. Lopez, M. Behrisch, L. Bieker-Walz, J. Erdmann, Y.-P. Flötteröd, R. Hilbrich, L. Lücken, J. Rummel, P. Wagner, and E. Wießner, "Microscopic traffic simulation using sumo," in *The 21st IEEE Int. Conference on Intelligent Transp. Systems*, IEEE, 2018.
- [21] D. Troullinos, G. Chalkiadakis, I. Papamichail, and M. Papageorgiou, "Lane-free microscopic simulation for connected and automated vehicles," in *Accepted in 2021 24th IEEE Int. Conference on Intelligent Transp.*, 2021.